01 Feb 2013

Particle Shape Enhances Specificity of Antibody-Displaying Nanoparticles

Sutapa Barua
Missouri University of Science and Technology, baruas@mst.edu

Jin-Wook Yoo

Poornima Kolhar

Aditya Wakankar

et. al. For a complete list of authors, see https://scholarsmine.mst.edu/che_bioeng_facwork/438

Recommended Citation

S. Barua et al., "Particle Shape Enhances Specificity of Antibody-Displaying Nanoparticles," *Proceedings of the National Academy of Sciences*, vol. 110, no. 9, pp. 3270-3275, National Academy of Sciences, Feb 2013.
The definitive version is available at https://doi.org/10.1073/pnas.1216893110

Particle shape enhances specificity of antibody-displaying nanoparticles

Sutapa Barua[a,1], Jin-Wook Yoo[b,1], Poornima Kolhar[a], Aditya Wakankar[c], Yatin R. Gokarn[c,2], and Samir Mitragotri[a,3]

[a]Department of Chemical Engineering, Center for Bioengineering, University of California, Santa Barbara, CA 93106; [b]College of Pharmacy, Pusan National University, Busan 609-735, South Korea; and [c]Pharmaceutical Development, Genentech, Inc., South San Francisco, CA 94080

Edited by Joseph M. DeSimone, The University of North Carolina, Chapel Hill, NC, and approved January 10, 2013 (received for review September 27, 2012)

Monoclonal antibodies are used in numerous therapeutic and diagnostic applications; however, their efficacy is contingent on specificity and avidity. Here, we show that presentation of antibodies on the surface of nonspherical particles enhances antibody specificity as well as avidity toward their targets. Using spherical, rod-, and disk-shaped polystyrene nano- and microparticles and trastuzumab as the targeting antibody, we studied specific and nonspecific uptake in three breast cancer cell lines: BT-474, SK-BR-3, and MDA-MB-231. Rods exhibited higher specific uptake and lower nonspecific uptake in all cells compared with spheres. This surprising interplay between particle shape and antibodies originates from the unique role of shape in determining binding and unbinding of particles to cell surface. In addition to exhibiting higher binding and internalization, trastuzumab-coated rods also exhibited greater inhibition of BT-474 breast cancer cell growth in vitro to a level that could not be attained by soluble forms of the antibody. The effect of trastuzumab-coated rods on cells was enhanced further by replacing polystyrene particles with pure chemotherapeutic drug nanoparticles of comparable dimensions made from camptothecin. Trastuzumab-coated camptothecin nanoparticles inhibited cell growth at a dose 1,000-fold lower than that required for comparable inhibition of growth using soluble trastuzumab and 10-fold lower than that using BSA-coated camptothecin. These results open unique opportunities for particulate forms of antibodies in therapeutics and diagnostics.

morphology | nanomedicine | nanotechnology | drug delivery

Antibodies are used routinely in various analytical, diagnostic, and therapeutic applications, including cell and protein sorting (1), in vitro assays (2), in vivo imaging (3), and targeted delivery of therapeutics for the treatment of various diseases, including cancer (4), arthritis (5), and allergies (6). Significant attention has been given to understanding the molecular basis of antibody–antigen interactions (7) as well as to molecular engineering of antibodies to enhance their functions (8). An increasingly larger number of emerging applications of antibodies, however, are based on particulate systems in which antibodies are chemically or physically immobilized on the surface of micro- or nanoparticles (9–11). Such particulate antibodies are being pursued for targeted drug delivery or imaging. Although the benefits of antibodies in delivering therapeutic carriers to tissues have long been recognized, the effect of carriers themselves on antibody function has been relatively less studied. The function of antibodies that are immobilized on particles depends on the physicochemical properties of underlying particles, including the choice of material, size, surface modification, and shape. Commonly used nanoparticles for immobilizing antibodies include gold (9), iron oxide (12), quantum dots (13, 14), silica (15), polymers including poly(lactide-coglycolic acid) (PLGA) (11, 16) and polystyrene (17, 18), liposomes (19), and albumin (20). Antibodies have been immobilized on these particles through physisorption as well as chemical conjugation (21), and it is known that particle size affects the interactions of immobilized antibodies with their targets (22, 23). However, the effect of particle shape, a key parameter of such interactions, is not known.

Here, we study the effect of shape using trastuzumab, a HER2 (human epidermal growth factor receptor 2)-targeting monoclonal antibody with proven therapeutic benefit (24) as a model antibody, polystyrene particles of two sizes (200 nm and 1 μm) and three shapes (spheres, rods, and disks) as model particles, and three breast cancer cell lines. We report a surprising finding: particle shape enhances avidity as well as specificity of interactions of antibodies with their targets. We further report, based on in vitro studies, that the shape-induced enhancement of specificity and avidity translates to large enhancements of therapeutic effect as judged by growth inhibition of $HER2^+$ breast cancer cells, BT-474.

Results

Preparation of Protein-Coated Particles with Three Different Shapes. Two sets of particles were prepared (Fig. 1*A*). The first set was prepared using 200-nm spheres. These spheres were stretched to prepare nanorods (367 ± 33 nm in length and 126 ± 8 nm in width) and nanodisks (236 ± 26 nm in diameter and 88 ± 21 nm in thickness). The second set of particles was prepared using microspheres (1 μm in diameter). These particles were stretched to prepare microrods (2.5 ± 0.28 μm in length and 0.68 ± 0.05 in width) and microdisks (1.39 ± 0.12 μm in diameter and 0.3 ± 0.06 μm in thickness). The surface of the particles was modified to elicit specific (trastuzumab) and nonspecific (BSA) interactions with cells. Trastuzumab and BSA were immobilized on the particle surface by adsorption, and the amounts adsorbed on their surface were quantified (Table S1). Detailed studies were performed using 200-nm spheres and corresponding rods. Desorption kinetics of trastuzumab and BSA from the surfaces of nanospheres and nanorods were studied in PBS buffer at pH 7.4 (Fig. S1 *A*, *i* and *ii*), and in 10% FBS containing PBS (Fig. S1 *B*, *i* and *ii*). A small fraction of protein desorbed from particles in 2 h (trastuzumab: 5–10% in PBS and 7–12% in FBS-PBS; BSA: 3–6% in PBS and 2–5% in FBS-PBS). The surface charge of nanospheres and nanorods (uncoated, trastuzumab-coated, and BSA-coated) was measured (Table S2). The mean zeta potentials of uncoated nanospheres and nanorods were approximately −20 mV in water, whereas the values increased to −9.5 and −9.3 mV, respectively, in 10% FBS containing cell culture medium. Adsorption of trastuzumab or BSA on nanoparticles further increased the zeta potential up to −5.3 mV.

Uptake of Nanoparticles by Breast Cancer Cells. We first compared intracellular uptake of three different shapes of particles (sphere, rod, and disk) in $HER2^+$ human breast cancer cells, BT-474, using confocal microscopy. The uptake of both uncoated and

Author contributions: S.B., J.-W.Y., P.K., A.W., Y.R.G., and S.M. designed research; S.B., J.-W.Y., and P.K. performed research; S.B., J.-W.Y., A.W., and Y.R.G. contributed new reagents/analytic tools; S.B., J.-W.Y., P.K., A.W., Y.R.G., and S.M. analyzed data; and S.B., J.-W.Y., A.W., Y.R.G., and S.M. wrote the paper.

The authors declare no conflict of interest.

This article is a PNAS Direct Submission.

[1]S.B and J.-W.Y. contributed equally to this work.

[2]Present address: Department of Chemical Engineering, Institute of Chemical Technology, Mumbai 400019, India.

[3]To whom correspondence should be addressed. E-mail: samir@engineering.ucsb.edu.

This article contains supporting information online at www.pnas.org/lookup/suppl/doi:10.1073/pnas.1216893110/-/DCSupplemental.

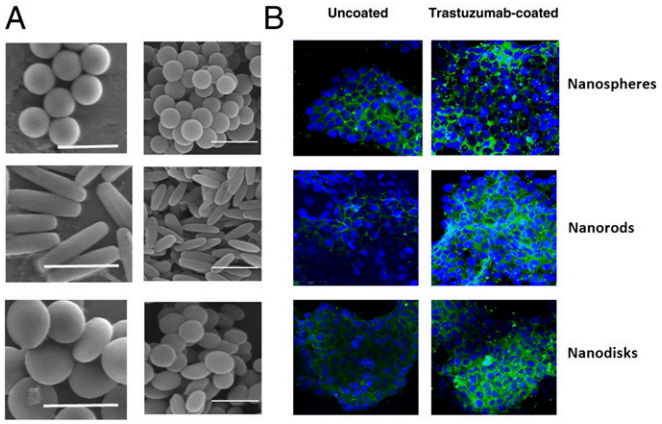

Fig. 1. Scanning electron micrographs of particles used in this study and images of their uptake in BT-474 cells. (*A*, *Left*) Microspheres, rods, and disks (scale: 2 μm). (*Right*) Nanospheres, rods, and disks. (Scale bar: 500 nm.) (*B*) Confocal micrographs of nanoparticle uptake in BT-474 cells. (*Left*) Nanoparticles without trastuzumab. (*Right*) Nanoparticles with trastuzumab.

trastuzumab-coated nano/microparticles was evaluated after 2 h incubation with BT-474 cells at 37 °C (Fig. 1*B*, *Left*: uncoated particles; Fig. 1*B*, *Right*: trastuzumab-modified particles). Uncoated nanospheres exhibited higher uptake in BT-474 cells compared with that exhibited by nanorods and nanodisks, implying that sphere is a favorable shape for cellular entry. When nanoparticles were coated with trastuzumab, uptake of all particles was increased. Interestingly, however, uptake of trastuzumab-coated nanoparticles exhibited different dependence on shape compared with that exhibited by uncoated nanoparticles. Nanorods and nanodisks, both of which exhibited lower uptake in BT-474 in the absence of trastuzumab, showed significantly higher uptake compared with spheres after trastuzumab coating. High-magnification confocal images confirmed that trastuzumab-coated nanorods and nanospheres are internalized by BT-474 cells (Fig. S2). Cell viability measurements evaluated using ethidium homodimer stain indicated that a 2-h exposure of BT-474, SK-BR-3, or MDA-MB-231 to trastuzumab-coated rods or spheres did not induce significant toxicity (Fig. S3).

Uptake of nanoparticles in BT-474 cells was quantified by recovering the nanoparticles from cells and measuring their fluorescence per milligram of total cellular protein contents (Fig. 2*A*). Consistent with the microscopic images, trastuzumab coating induced a higher enhancement of uptake of rods and disks compared with their spherical counterparts (black bar). Overall, trastuzumab-coated nanorods exhibited the highest uptake in BT-474 cells. Uptake of trastuzumab-coated nanoparticles in BT-474 cells was reduced when the cells were preincubated with excess trastuzumab before addition of nanoparticles (hatched bar), thus confirming the specific nature of nanoparticle uptake. BSA-coated nanoparticles exhibited low uptake (crossed bar), further confirming the role of trastuzumab in nanoparticle uptake.

To assess the role of trastuzumab–cell interactions in nanoparticle uptake, nanoparticle internalization was evaluated in two additional cell lines: SK-BR-3, a $HER2^+$ cell line, and MDA-MB-231, a $HER2^-$ cell line. The extent of uptake in SK-BR-3 cells was lower than that seen in BT-474 cells for all nanoparticles (Fig. 2*B*). However, nanorods exhibited significantly higher uptake compared with spheres. In addition, preincubation of cells with trastuzumab (hatched bar) once again reduced the uptake of trastuzumab-coated nanorods (black bar) to the same level as that exhibited by uncoated nanorods (open bar). $HER2^-$ MDA-MB-231 cells did not exhibit trastuzumab-mediated enhancement of cellular uptake of nanoparticles, regardless of particle shape (Fig. 2*C*).

The dependence of trastuzumab-induced nanoparticle uptake on shape and cell type is summarized in Fig. 3*A*. Spheres exhibited the least enhancement of nanoparticle uptake in the presence of trastuzumab. The highest enhancement for spheres, about twofold, was observed for BT-474 cells, whereas no enhancement was observed for MDA-MB-231 cells. Rods exhibited the highest enhancement in the presence of trastuzumab: about sixfold for BT-474, 2.5-fold for SK-BR-3, and none for MDA-MB-231. Disks also exhibited high enhancement due to trastuzumab: about fivefold for BT-474, twofold for SK-BR-3, and none for MDA-MB-231. Results of similar measurements performed for microparticles are shown in Fig. 3*B*. The dependence of trastuzumab-mediated enhancement on particle shape was much more prominent for microparticles than that for 200-nm nanoparticles. A high enhancement of 15-fold was observed for microrod uptake by SK-BR-3 cells.

Particle Shape Affects Specific and Nonspecific Uptake. Particle shape exhibits unique interdependence with target specificity. Fig. 3*C* depicts the ratio of rods and spheres internalized by BT-474, SK-BR-3, or MDA-MB-231 cells under various conditions, including four specific conditions (trastuzumab in BT-474 and SK-BR-3 for 200 nm and 1 μm) and various nonspecific conditions (uncoated particles in BT-474, SK-BR-3, and MDA-MB-231 cells for 200 nm and 1 μm; BSA-coated particles in BT-474, SK-BR-3, and MDA-MB-231 cells for 200 nm; trastuzumab-coated particles in MDA-MB-231 cells for 200 nm and 1 μm; and trastuzumab-coated particles in BT-474, SK-BR-3, and MDA-MB-231 cells for 200 nm when blocked with excess trastuzumab). Remarkably, for all specific cases, rods exhibited higher uptake compared with spheres. The mean ratio for specific uptake of rods to spheres was 1.6. Conversely, for all nonspecific cases, rods exhibited lower uptake compared with spheres, with a mean ratio of 0.68. A similar observation was made for disks, although the magnitude of this effect was lower compared with rods (Fig. 3*D*).

Shape-Specific Enhancement of Nanoparticle Uptake: Role of Attachment. We hypothesized that the enhancement in intracellular uptake of trastuzumab-coated nano/microrods over their spherical counterparts originated from enhanced binding of trastuzumab-coated rods to the cell membrane compared with spheres. To test this hypothesis, concentration-dependent cell-surface binding of trastuzumab-coated nanorods, trastuzumab-coated nanospheres, uncoated rods, and uncoated spheres was assessed in BT-474 cells at 4 °C. This temperature was chosen to

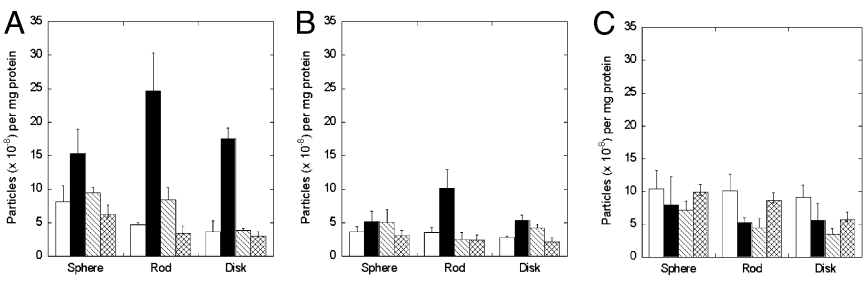

Fig. 2. Nanoparticle uptake in BT-474 (*A*), SK-BR-3 (*B*), and MDA-MB-231 (*C*) cells. Open bars, nanoparticles with no trastuzumab on the surface; black bars, nanoparticles with trastuzumab on the surface; hatched bars, trastuzumab-coated nanoparticles exposed to cells after preincubation with trastuzumab; crossed bars, BSA-coated particles. Nanoparticle dimensions are as shown in Fig 1*A*, *Right*. Cells were incubated with a nanoparticle concentration of 300 μg/mL in all experiments. Data expressed as mean ± SD (n = 4).

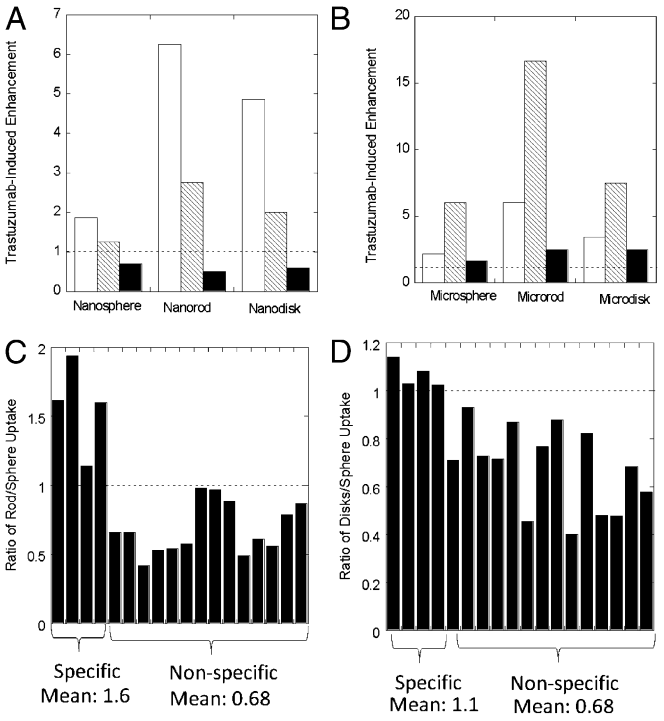

Fig. 3. Trastuzumab-induced enhancement of nano- and microparticle uptake by various cell lines used in this study. The *y* axis corresponds to uptake of trastuzumab-coated particles divided by uptake of uncoated particles of same size/shape in the same cells. (*A*) Uptake of nanoparticles for BT-474 (white bars), SK-BR-3 (hatched bars), and MDA-MB-231 (black bars). Particle concentration in all experiments was 300 μg/mL. (*B*) Similar data for microparticles. Particle concentration in all experiments in *B* was 300 μg/mL. (*C* and *D*) Ratio of rod/sphere (*C*) and disk/sphere (*D*) uptake ratio for various particles and cell conditions used in this study. The conditions are classified as specific or nonspecific. The specific conditions include trastuzumab-coated nano- and microparticles in BT-474 and SK-BR-3 (a total of four conditions). The nonspecific conditions include uncoated nano- and microparticles in BT-474, SK-BR-3, and MDA-MB-231 (a total of six conditions); BSA-coated nanoparticles in BT-474, SK-BR-3, and MDA-MB-231 (three conditions); trastuzumab-coated nano- and microparticles in MDA-MB-231 cells (two conditions); and trastuzumab-coated nanoparticles in BT-474, SK-BR-3, and MDA-MB-231 cells, when blocked with excess trastuzumab (three conditions). Altogether, a total of fourteen nonspecific conditions are included. The same conditions are used for rods and disks.

prevent cellular internalization of nanoparticles. Trastuzumab-coated nanorods exhibited a higher degree of binding than coated nanospheres, uncoated nanospheres, and uncoated nanorods (Fig. 4*A*). The mean fluorescence intensity of bound nanorods increased with nanorod concentration and reached a saturation point after which addition of more particles did not increase further binding. A similar behavior was observed for trastuzumab-coated nanospheres. The uncoated nanorods and nanospheres showed minimal attachment at concentrations ≤5 μg/mL. At higher concentrations, binding of uncoated nanoparticles to the cell membrane increased slightly and reached saturation, although the magnitude was significantly lower than that for trastuzumab-coated particles. A further increase in particle concentration to 300 μg/mL did not induce an additional drop in binding (Table S4).

Fig. 4*B* shows the area-under-the-curve (AUC) values of fluorescence intensity vs. concentration from Fig. 4*A*. The secondary *y* axis of Fig. 4*B* is redrawn from Fig. 2*A* and represents the number of nanoparticle uptakes by BT-474 cells following 2 h incubation. The close resemblance between binding AUC values and internalization suggests that the peculiar interplay between shape and specificity may have originated from binding to cell surface.

Significance of Rod-Shaped Nanoparticles to Optimize Therapeutic Effect. Because trastuzumab is a therapeutic antibody, enhanced binding of trastuzumab-coated nanoparticles is expected to provide direct therapeutic benefits. To assess this possibility, we measured the ability of trastuzumab-coated nanorods and nanospheres to inhibit growth of BT-474 cells (Fig. 5*A*). Trastuzumab-coated nanorods (Fig. 5*A*, black bars) induced significantly higher inhibition of growth compared with that induced by the same amount of trastuzumab delivered in the soluble form (Fig. 5*A*, gray bars). Enhanced growth inhibition was seen in a dose-dependent manner at nanorod concentrations from 0.1 to 10 μg/mL (corresponding to trastuzumab concentrations from 0.016 to 1.25 μg/mL). The inhibitory effect of trastuzumab-coated nanorods on BT-474 cells cannot be attributed to rods themselves, because the same dose of polystyrene nanorods, when coated with BSA, did not induce a detectable effect on growth inhibition (Fig. 5*A*, hatched bars). Trastuzumab-coated nanospheres (crossed bars) failed to induce appreciable growth inhibition and produced a result comparable to that of BSA-coated nanospheres (open bars). This limited growth inhibition induced by BSA-coated nanospheres might have originated from nonspecific internalization. Such minor effects of polystyrene nanoparticles are consistent with literature reports (25, 26).

The model polymer, polystyrene, may be replaced by biocompatible polymer poly-l-lactide co-glycolide (PLGA). PLGA particles with dimensions comparable to those of polystyrene particles reported in Fig. 1*A* may be prepared (Fig. S4 and *SI Text*, section 4). The ability of trastuzumab-coated nanorods to induce growth inhibition may be enhanced further by encapsulating a chemotherapeutic drug in PLGA nanorods or entirely replacing the polymer with the drug. Here, we demonstrate the feasibility of this approach by preparing nanorods of comparable dimensions using a chemotherapeutic drug, camptothecin (Fig. 5*B*, see *SI Text*, sections 1, 2, and 3, and Table S3 for preparation, trastuzumab coating, and characterization). Trastuzumab-coated camptothecin nanorods (Fig. 5*C*, black bars) exhibited higher growth inhibitory effects in BT-474 cells than trastuzumab-coated polystyrene nanorods (Fig. 5*A*, black bars) and BSA-coated camptothecin (Fig. 5*C*, hatched bars). For example, 50% inhibition of growth required 1.25 μg/mL trastuzumab on 10 μg/mL polystyrene nanorods or 10 μg/mL BSA-coated camptothecin. In contrast, the same inhibition was obtained using only 0.16 μg/mL trastuzumab coated on 1 μg/mL camptothecin. Similarly, 30% growth inhibition was observed using only 0.016 μg/mL trastuzumab coated on 0.1 μg/mL camptothecin; this number was 10-fold lower than the required dose of BSA-coated camptothecin (1 μg/mL). Exposure to trastuzumab alone at the concentrations comparable to those exposed from the nanorods (Fig. 5*C*, gray bars) did not induce inhibition comparable to that induced by trastuzumab-coated camptothecin. The effect of trastuzumab-coated camptothecin was cell-line dependent; comparable inhibition was found in $HER2^+$ cell lines, BT-474 and SK-BR-3, but no enhanced cell growth inhibition was found in a $HER2^-$ cell line, MDA-MB-231 (Fig. S5).

Discussion

Studies reported here show that binding and subsequent cellular uptake of antibody- coated nanoparticles is shape dependent. Nanoparticle uptake without trastuzumab coating may be a result of nonspecific binding interactions, e.g., hydrophobic binding of polystyrene nanoparticles at the cell membrane (27). In case of specific interactions, trastuzumab-coated nanorods showed the highest uptake and surface binding to $HER2^+$ cells, that is, BT-474 and SK-BR-3, and negligible binding to $HER2^-$ MDA-MB-231 cells (Fig. 3). HER2 expression is expected to be higher in BT-474 cells than in other breast cancer cell lines (28), which may explain the highest uptake of trastuzumab-coated nanoparticles in these cells. The magnitude of trastuzumab-coated particle uptake and cellular internalization generally was highest for rods, followed by disks, followed by spheres. The enhanced uptake of rods is consistent with the results reported by Gratton

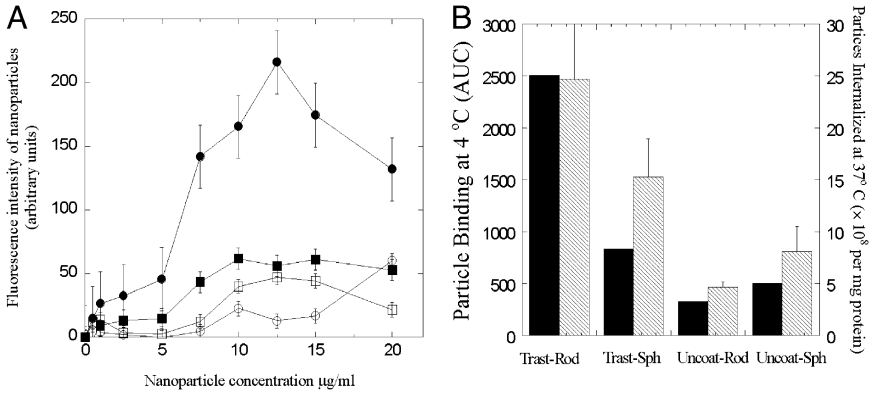

Fig. 4. (*A*) Concentration-dependent binding of nanoparticles to BT-474 at 4 °C after incubation for 30 min. ●, Trastuzumab-coated nanorods (Trast-Rod); ○, uncoated nanorods (Uncoat-Rod); ■, trastuzumab-coated nanospheres (Trast-Sph); □, uncoated nanospheres (Uncoat-Sph). Data were expressed as mean ± SD (n = 4). (*B*) AUC of nanoparticles attached to BT-474 (black bars) and the number of nanoparticles taken up by BT-474 (hatched bars) taken from Fig. 2 are shown in the primary and secondary y axes, respectively.

et al. (29), which showed that poly(ethylene glycol) hydrogel rods of 150 × 450 nm exhibit higher uptake compared with cylindrical particles of 200 × 200 nm. In their study, the interaction between the particles and the membrane was mediated by the positive charge of the particle. Elimination of the positive charge eliminated enhanced uptake. In our study, particle–membrane interactions were mediated by trastuzumab. Trastuzumab-coated nanorods exhibited about sixfold higher uptake compared with uncoated nanorods in BT-474 cells. The enhancement was even higher for microrods, in which a 15-fold enhancement was observed in the uptake of microrods in SK-BR-3 cells. Corresponding enhancement for spherical particles was about twofold and fivefold, respectively, thus confirming the role of shape in increased uptake. The most unexpected conclusion of the studies, however, is that particle shape enhances specificity of binding and uptake. Compared with spheres, rods exhibited, on average, 1.6-fold higher uptake when the uptake was specific and about 1.5-fold lower uptake when the uptake was nonspecific. Collectively, these results show that the specificity of trastuzumab-mediated binding and uptake was enhanced by about 2.3-fold. This simultaneous enhancement in affinity and specificity is a highly unique contribution of particle morphology.

Trastuzumab attachment previously was shown to increase internalization of nanoparticles by $HER2^+$ cells. For example, about 1.4 to 4-fold enhancement in internalization of 100 nm iron oxide nanoparticles has been reported in SK-BR-3 cells (30, 31). Other studies have reported a 1.4-fold improvement in cytotoxicity of chitosan nanoparticles in an ovarian carcinoma continuous cell line, SKOV-3 (32); 1.2–1.3-fold enhancement in uptake of polylactic acid (PLA) or PLGA nanoparticles by SK-BR-3 cells (11, 33, 34); and 2–3-fold increase in uptake of albumin nanoparticles by BT-474 and SK-BR-3 cells (20). The enhancements in uptake reported here, 6-fold for nanorods and 15-fold for microrods, compare favorably with these numbers.

High uptake of trastuzumab-coated rods may have originated from multivalent interactions of trastuzumab with HER2, which also may explain their highest attachment to cell surface (Fig. 4*A*). Rods offer higher surface area per unit volume compared with spheres and therefore can adsorb higher amounts of trastuzumab. Theoretically, the surface area/volume ratio of a nanorod (126 × 367 nm), calculated using standard equations for determining areas and volumes of prolate ellipsoids, is about 31% higher than that for a sphere (200-nm diameter). The amount of trastuzumab adsorbed on rods was about 24% higher than that on spheres (Table S1), indicating that the surface density of trastuzumab on rods and spheres was comparable. The magnitude of membrane binding, on the other hand, differed by ∼300% (Fig. 4*B*).The bell-shaped curve for trastuzumab-coated nanorods might be a result of multivalent binding and consequent cross-linking of HER2. Such effects previously were reported based on experiments and theory (35, 36). Multivalent gold nanoparticles coated with dinitrophenyl have shown a similar bell-shaped dose–response curve due to cross-linking of IgE-FcεRI receptor complexes in RBL-2H3 mast cells (37). Although the studies presented here suggest that enhanced uptake of nanorods can be explained by enhanced surface binding, additional factors associated with multivalent interactions and penetration through the glycocalyx also are likely explanations for the experimental observations (*SI Text*, section 5).

The enhanced specificity might have originated from the interplay between binding interactions of particles with cell surface and the forces of their detachment, both of which likely depend on shape. The probability of adhesion of a particle on a surface, P, is given by the following expression (38, 39):

$$P \cong m_1 m_2 K_m^0 A_c \exp\left[-\frac{\lambda f}{k_B T}\right], \qquad [1]$$

where K_m^0 is the equilibrium binding constant for the antibody–receptor bond; m_1 and m_2 are surface densities of receptors and antibodies, respectively; A_c is the contact area of the particle; λ is

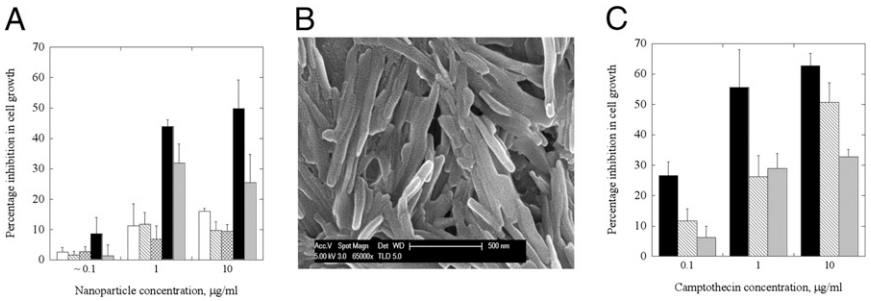

Fig. 5. Effect of trastuzumab-coated nanoparticles on cell growth inhibition. (*A*) BT-474 cells exposed to three different concentrations of trastuzumab-coated nanorods or nanospheres (black bars and crossed bars, respectively), BSA-coated nanorods or nanospheres (hatched and open bars, respectively), or trastuzumab solution alone (gray bars). Percentage growth inhibition assay was performed using a live/dead assay kit (Invitrogen) and expressed as a percentage of control cells incubated with PBS. Average values and SDs of four replicates are reported. Results show that trastuzumab-coated nanorods significantly enhance the growth inhibition, whereas trastuzumab alone fails to improve the growth inhibition. (*B*) SEM images of camptothecin nanoparticles as prepared by the solvent diffusion method. The mean length of the nanoparticles is 509.5 ± 202.6 nm. (*C*) Comparison of inhibition in cell growth following treatment with trastuzumab-coated camptothecin (black bars), BSA-coated camptothecin (hatched bars), or trastuzumab alone (gray bars) in BT-474 cells. The data represent mean ± SD (n = 4).

the bond interaction parameter and may be represented as the distance at which the adhesion force reduces to zero; f is the external force experienced by each of the individual bonds during detachment; and k_B and T are Bolzmann's constant and temperature in kelvins, respectively. A semiquantitative analysis of Eq. **1** yields the equations for relative probability of adhesion for rods and spheres, $\frac{P_{rod}}{P_{sph}}$, as follows (see *SI Text*, section 6 for details):

For specific interactions, that is, $\lambda \to 0$,

$$\frac{P_{rod}}{P_{sph}} \cong \alpha^m. \quad [2]$$

For nonspecific interactions, that is, $\lambda \to \infty$,

$$\frac{P_{rod}}{P_{sph}} \cong 0. \quad [3]$$

This simple analysis provides a possible explanation for the observed behavior. In the presence of specific antibodies (Eq. **2**), rods exhibit higher adhesion, primarily owing to their increased contact area with the surface, which increases with increasing α.

Multivalent interactions also affected biological effects of trastuzumab-coated polystyrene or camptothecin nanorods in terms of their ability to inhibit the growth of breast cancer cells (39). Exposure to the same amount of trastuzumab from solution and nanorods produced significantly different effects on cell growth (Fig. 5*A*). More importantly, the effect of trastuzumab-coated nanorods on growth inhibition could not be matched by trastuzumab solution, even at higher doses. Specifically, trastuzumab-coated polystyrene nanorods induced ~50% inhibition at a trastuzumab concentration of 1.25 μg/mL, whereas soluble trastuzumab alone produced only a 31.9 ± 4.2% inhibition, even at a 20-fold higher concentration (25 μg/mL), a concentration within the therapeutic range (40). Use of pure chemotherapeutic drug nanoparticles further enhanced the effect of trastuzumab; 0.016 and 0.16 μg/mL trastuzumab on 0.1 and 1 μg/mL camptothecin, respectively, inhibited 30% and 50% growth, respectively. The same levels of growth inhibition require 10-fold higher concentrations of BSA-coated camptothecin. Such effects may enhance the efficacy of existing applications or may open new opportunities for antibodies. Particle shape may affect additional properties of antibodies on the surface, including their desorption and substitution by immunoglobulins in the body, and this likelihood needs further evaluation (41).

The combination of reduced nonspecific binding and enhanced specific binding has several applications. For drug delivery applications, this observation provides a direct benefit for enhanced targeting. This report describes in vitro studies, and confirmation of these results in vivo is required before applications in drug delivery can be considered further. However, the behavior of nanoparticles in vivo is dictated by several factors, including circulation, immune clearance, flow, and extravasation, which makes it difficult to interpret the contribution of specific and nonspecific binding of nanoparticles to target cells (42). This makes the present study especially significant because it provides a detailed quantitative analysis of interplay between shape and specificity, which offers principles for drug carrier design. Enhancement of specific binding also may open applications in imaging, in which antibody-coated nanoparticles are used in vitro for imaging cancer cells using antibody-coated fluorescent nanoprobes (14). Antibody-coated nano/microrods also may be used for the development of bioaffinity assays for in vitro diagnostic applications. Rod-shaped nanoparticles may potentially improve the sensitivity of traditional nanoparticle-based agglutination and lateral flow assays that suffer from weak antigen–antibody attachment and nonspecific binding (43). Overall, it is envisioned that the shape-specific nanoparticles will have versatile implications in the field of therapeutics and diagnostics.

Methods

Materials. Fluorescent polystyrene particles (Fluoresbrite) with diameter of 200 nm and 1 μm were purchased from Polysciences, Inc. RPMI medium 1640, McCoy's 5A medium, and FBS were purchased from ATCC. DMEM, L-glutamine, and insulin were purchased from Invitrogen. Trastuzumab was provided by Genentech, Inc. BSA was purchased from Sigma-Aldrich. All other reagents were the highest possible commercial grade available.

Preparation and Characterization of Protein-Coated Particles. Polystyrene rod- and disk-shaped particles were prepared from polystyrene spherical particles using the film-stretching procedure described by our previous reports (44, 45). The mean zeta potentials of uncoated and protein-coated polystyrene nanoparticles were determined by dynamic light scattering using a Malvern Zetasizer Nanoseries. Samples of 50 μg/mL were prepared in 1 mL of filter sterile PBS or cell culture medium and placed in a capillary cell. Zeta potential measurement of each sample consisted of at least 15 runs. The results of two independent sets of each sample were expressed as mean zeta potential ± SD.

Cell Culture. BT-474 cells were cultured in RPMI 1640 medium supplemented with 10% FBS, 1% penicillin–streptomycin, and 10 μg/mL insulin. SK-BR-3 cells were cultivated in McCoy's 5A medium supplemented with 10% FBS, 1% penicillin–streptomycin, and 2 mM L-glutamine. MDA-MB-231 cells were grown in complete growth medium containing DMEM, 10% FBS, and 1% penicillin–streptomycin. All the cell lines were incubated at 37 °C in a humidified chamber with 5% CO_2 and cultured in exponential growth phase by subcultivation.

Confocal Microscopy. For confocal microscopy, BT-474 cells were seeded on cover glasses and cultured in RPMI 1640 medium as above until reading 80% confluency. Cells were incubated with 0.1 mg of nanoparticles for 2 h at 37 °C and were washed several times with cold HBSS, followed by cell boundary staining using CellMask Deep Red membrane dye (Invitrogen) at 5 μg/mL for 5 min at 37 °C, five washings, and fixing with 4% paraformaldehyde at room temperature for 10 min. The cells were washed with PBS three times and incubated with 0.2% Triton X-100 for 5 min. The nucleus was stained with DAPI (2 μg/mL) for 5 min. The cover glasses were placed on a slide glass using Permount mounting medium (Fisher Scientific). The samples were imaged on a confocal microscope (Leica and Olympus FluoView 500).

Cellular Uptake Study. Cells were seeded in 24-well plates. When cells reached 80% confluency, they were gently washed three times using HBSS buffer and incubated with 0.3 mL medium; 0.1 mg of nanoparticles or microparticles was added to the wells. Cells were incubated for 2 h at 37 °C. Cells were washed using cold HBSS to stop the uptake and washed three more times to remove unbound and surface-bound particles. After lysis with Triton X-100 (1% in 0.1 M NaOH), protein was analyzed using a Pierce Micro BCA protein kit (Thermo Scientific) and the amount of particles internalized was calculated using a Tecan Infinite microplate reader at excitation and emission wavelengths of 425 nm and 465 nm, respectively.

Cell Viability. To evaluate the cytotoxicity of the nanoparticles, BT-474, SK-BR-3, and MDA-MB-231 cells were grown overnight at a density of 10,000 cells per 0.2 mL in 96-well plates. Cells were incubated for 2 h at 37 °C with 300 μg/mL trastuzumab-coated nanospheres, trastuzumab-coated nanorods, uncoated nanospheres, or uncoated nanorods. Dead cells were stained with 2 μM ethidium homodimer-1 (EthD-1; Invitrogen) by incubating the cells for 30 min at room temperature. The fluorescence intensity of EthD-1 was measured using 495/645 excitation/emission filters of a microplate reader (Tecan). Background fluorescence of the cells treated with PBS was subtracted from the samples. The percentage cell viability was calculated by subtracting the dead cells from 100% live cells.

Binding of Trastuzumab-Coated Nanospheres and Nanorods with BT-474. BT-474 cells were seeded in 96-well plates at a concentration of 8,400 cells per well and allowed to grow overnight. The cells were incubated at 4 °C for 30 min with various concentrations of trastuzumab-coated nanorods and nanospheres in a range of 0–20 μg/mL and at 300 μg/mL. Cells were washed using PBS after removal of the nanoparticles, fixed using 4% paraformaldehyde for 15 min at room temperature (~22 °C), washed using PBS, and kept in 150 μL PBS per well. Fluorescence intensities of the nanoparticles from each well were measured using a Tecan Infinite microplate reader at excitation and emission wavelengths of 425 nm and 465 nm, respectively. The half-maximum particle-binding concentration was calculated from the dose–response curve of fluorescence intensity vs. particle concentration where 50% of the

maximum fluorescence intensity was found. The data were obtained for two independent sets of experiments with four replicates of each concentration.

Inhibition in Cancer Cell Growth Using Trastuzumab-Coated Polystyrene Nanoparticles. The therapeutic efficiency of trastuzumab was examined in BT-474 cells in vitro using trastuzumab-coated nanorods and trastuzumab-coated nanospheres. BSA-coated nanoparticles and trastuzumab alone were used as controls. BT-474 cells were grown in 24-well plates and treated with nanoparticles (0.13, 1, and 10 μg/mL polystyrene rods or spheres) or controls (trastuzumab concentrations on rods were 0.016, 0.125, and 1.25 μg/mL, respectively, and on spheres were 0.013, 0.1, and 1 μg/mL, respectively) for 2 h. Cells then were incubated with fresh serum containing medium and allowed to grow for an additional 94 h. After the treatments, live and dead cells were quantified using calcein-AM and EthD-1 (live/dead assay, Invitrogen), respectively. Fluorescence intensities of calcein-AM [excitation/emission (Ex/Em): 495/530] and EthD-1 (Ex/Em: 495/645) were measured using a plate reader (Tecan). Fluorescence background of medium was subtracted from each well. Total numbers of live and dead cells were calculated from standard curves of fluorescence intensities vs. number of live/dead cells. The data were expressed as percentage inhibition in cell proliferation (or number of live cells) compared with PBS-treated controls.

ACKNOWLEDGMENTS. We thank Mark Cornish for his help with SEM, which was supported by the Materials Research Science and Engineering Centers program of the National Science Foundation (Award MR05-20415); and Dr. Mary Raven for her help with confocal microscope facility, which was supported by National Institutes of Health Grant 1 S10 OD010610-01A1. This work was supported by a grant from Genentech Inc. and University of California's UC Discovery grants program. S.B. acknowledges the Daryl and Marguerite Errett Discovery Award in Biomedical Research.

1. Ward ES, Ober RJ (2009) Multitasking by exploitation of intracellular transport functions: The many faces of FcRn. *Advances in Immunology*, ed Alt FW (Academic, San Diego), 103, pp 77–115.
2. Haab B, Dunham M, Brown P (2001) Protein microarrays for highly parallel detection and quantitation of specific proteins and antibodies in complex solutions. *Genome Biol* 2(2):RESEARCH0004.
3. Valadon P, et al. (2010) Designed auto-assembly of nanostreptabodies for rapid tissue-specific targeting in vivo. *J Biol Chem* 285(1):713–722.
4. Burris HA, 3rd, et al. (2011) Phase II study of the antibody drug conjugate trastuzumab-DM1 for the treatment of human epidermal growth factor receptor 2 (HER2)-positive breast cancer after prior HER2-directed therapy. *J Clin Oncol* 29(4): 398–405.
5. Emery P, et al. (2008) Comparison of methotrexate monotherapy with a combination of methotrexate and etanercept in active, early, moderate to severe rheumatoid arthritis (COMET): A randomised, double-blind, parallel treatment trial. *Lancet* 372(9636): 375–382.
6. Corren J Anti-interleukin-5 antibody therapy in asthma and allergies*Curr Opin Allergy Clin Immunol*(2011) 116565–570, 10.1097/ACI.1090b1013e32834c32833d32830.
7. Sundberg EJ (2009) Structural basis of antibody-antigen interactions. *Methods Mol Biol* 524:23–36.
8. Cuesta ÁM, Sainz-Pastor N, Bonet J, Oliva B, Álvarez-Vallina L (2010) Multivalent antibodies: When design surpasses evolution. *Trends Biotechnol* 28(7):355–362.
9. Choi CHJ, Alabi CA, Webster P, Davis ME (2010) Mechanism of active targeting in solid tumors with transferrin-containing gold nanoparticles. *Proc Natl Acad Sci USA* 107(3): 1235–1240.
10. Kocbek P, Obermajer N, Cegnar M, Kos J, Kristl J (2007) Targeting cancer cells using PLGA nanoparticles surface modified with monoclonal antibody. *J Control Release* 120(1-2):18–26.
11. Sun B, Ranganathan B, Feng S-S (2008) Multifunctional poly(D,L-lactide-co-glycolide)/montmorillonite (PLGA/MMT) nanoparticles decorated by Trastuzumab for targeted chemotherapy of breast cancer. *Biomaterials* 29(4):475–486.
12. Chen T-J, et al. (2009) Targeted Herceptin-dextran iron oxide nanoparticles for noninvasive imaging of HER2/neu receptors using MRI. *J Biol Inorg Chem* 14(2):253–260.
13. Wu X, et al. (2003) Immunofluorescent labeling of cancer marker Her2 and other cellular targets with semiconductor quantum dots. *Nat Biotechnol* 21(1):41–46.
14. Gao X, Cui Y, Levenson RM, Chung LWK, Nie S (2004) In vivo cancer targeting and imaging with semiconductor quantum dots. *Nat Biotechnol* 22(8):969–976.
15. Tsagkogeorgas F, Ochsenkühn-Petropoulou M, Niessner R, Knopp D (2006) Encapsulation of biomolecules for bioanalytical purposes: Preparation of diclofenac antibody-doped nanometer-sized silica particles by reverse micelle and sol-gel processing. *Anal Chim Acta* 573-574(0):133–137.
16. Sahoo SK, Labhasetwar V (2005) Enhanced antiproliferative activity of transferrin-conjugated paclitaxel-loaded nanoparticles is mediated via sustained intracellular drug retention. *Mol Pharm* 2(5):373–383.
17. Napp J, et al. (2011) Targeted luminescent near-infrared polymer-nanoprobes for in vivo imaging of tumor hypoxia. *Anal Chem* 83(23):9039–9046.
18. Butler JE, Lü EP, Navarro P, Christiansen B (1997) Comparative studies on the interaction of proteins with a polydimethylsiloxane elastomer. I. Monolayer protein capture capacity (PCC) as a function of protein pI, buffer pH and buffer ionic strength. *J Mol Recognit* 10(1):36–51.
19. Gupta B, Torchilin VP (2007) Monoclonal antibody 2C5-modified doxorubicin-loaded liposomes with significantly enhanced therapeutic activity against intracranial human brain U-87 MG tumor xenografts in nude mice. *Cancer Immunol Immunother* 56(8): 1215–1223.
20. Steinhauser I, Spänkuch B, Strebhardt K, Langer K (2006) Trastuzumab-modified nanoparticles: Optimisation of preparation and uptake in cancer cells. *Biomaterials* 27(28):4975–4983.
21. Shenton W, Davis SA, Mann S (1999) Directed self-assembly of nanoparticles into macroscopic materials using antibody–antigen recognition. *Adv Mater* 11(6):449–452.
22. Jiang W, Kim BY, Rutka JT, Chan WC (2008) Nanoparticle-mediated cellular response is size-dependent. *Nat Nanotechnol* 3(3):145–150.
23. Zhang S, Li J, Lykotrafitis G, Bao G, Suresh S (2009) Size-dependent endocytosis of nanoparticles. *Adv Mater* 21(4):419–424.
24. Slamon DJ, et al. (1987) Human breast cancer: Correlation of relapse and survival with amplification of the HER-2/neu oncogene. *Science* 235(4785):177–182.
25. Clift MJ, Bhattacharjee S, Brown DM, Stone V (2010) The effects of serum on the toxicity of manufactured nanoparticles. *Toxicol Lett* 198(3):358–365.
26. Smith PJ, et al. (2012) Cellular entry of nanoparticles via serum sensitive clathrin-mediated endocytosis, and plasma membrane permeabilization. *Int J Nanomedicine* 7:2045–2055.
27. Nel AE, et al. (2009) Understanding biophysicochemical interactions at the nano-bio interface. *Nat Mater* 8(7):543–557.
28. Szöllösi J, Balázs M, Feuerstein BG, Benz CC, Waldman FM (1995) ERBB-2 (HER2/neu) gene copy number, p185HER-2 overexpression, and intratumor heterogeneity in human breast cancer. *Cancer Res* 55(22):5400–5407.
29. Gratton SE, et al. (2008) The effect of particle design on cellular internalization pathways. *Proc Natl Acad Sci USA* 105(33):11613–11618.
30. Mi Y, Liu X, Zhao J, Ding J, Feng SS (2012) Multimodality treatment of cancer with herceptin conjugated, thermomagnetic iron oxides and docetaxel loaded nanoparticles of biodegradable polymers. *Biomaterials* 33(30):7519–7529.
31. Wuang SC, Neoh KG, Kang ET, Pack DW, Leckband DE (2008) HER-2-mediated endocytosis of magnetic nanospheres and the implications in cell targeting and particle magnetization. *Biomaterials* 29(14):2270–2279.
32. Yousefpour P, Atyabi F, Vasheghani-Farahani E, Movahedi AA, Dinarvand R (2011) Targeted delivery of doxorubicin-utilizing chitosan nanoparticles surface-functionalized with anti-Her2 trastuzumab. *Int J Nanomedicine* 6:1977–1990.
33. Koopaei MN, et al. (2011) Docetaxel immunonanocarriers as targeted delivery systems for HER 2-positive tumor cells: Preparation, characterization, and cytotoxicity studies. *Int J Nanomedicine* 6:1903–1912.
34. Liu J, Li J, Rosol TJ, Pan X, Voorhees JL (2007) Biodegradable nanoparticles for targeted ultrasound imaging of breast cancer cells in vitro. *Phys Med Biol* 52(16): 4739–4747.
35. Perelson AS (1981) Receptor clustering on a cell surface. III. Theory of receptor cross-linking by multivalent ligands: description by ligand states. *Math Biosci* 53(1–2):1–39.
36. Sulzer B, Perelson AS (1996) Equilibrium binding of multivalent ligands to cells: Effects of cell and receptor density. *Math Biosci* 135(2):147–185.
37. Huang Y-F, Liu H, Xiong X, Chen Y, Tan W (2009) Nanoparticle-mediated IgE-receptor aggregation and signaling in RBL mast cells. *J Am Chem Soc* 131(47):17328–17334.
38. Piper JW, Swerlick RA, Zhu C (1998) Determining force dependence of two-dimensional receptor-ligand binding affinity by centrifugation. *Biophys J* 74(1):492–513.
39. Decuzzi P, Ferrari M (2006) The adhesive strength of non-spherical particles mediated by specific interactions. *Biomaterials* 27(30):5307–5314.
40. Tokuda Y, et al. (1999) Dose escalation and pharmacokinetic study of a humanized anti-HER2 monoclonal antibody in patients with HER2/neu-overexpressing metastatic breast cancer. *Br J Cancer* 81(8):1419–1425.
41. Gessner A, Lieske A, Paulke B-R, Müller RH (2003) Functional groups on polystyrene model nanoparticles: Influence on protein adsorption. *J Biomed Mater Res A* 65(3):319–326.
42. Albanese A, Tang PS, Chan WCW (2012) The effect of nanoparticle size, shape, and surface chemistry on biological systems. *Annu Rev Biomed Eng* 14(1):1–16.
43. Luchini A, Longo C, Espina V, Petricoin EF, 3rd, Liotta LA (2009) Nanoparticle technology: Addressing the fundamental roadblocks to protein biomarker discovery. *J Mater Chem* 19(29):5071–5077.
44. Champion JA, Mitragotri S (2006) Role of target geometry in phagocytosis. *Proc Natl Acad Sci USA* 103(13):4930–4934.
45. Champion JA, Katare YK, Mitragotri S (2007) Making polymeric micro- and nanoparticles of complex shapes. *Proc Natl Acad Sci USA* 104(29):11901–11904.